

Catalytic Formation of Narrow Nb Nanowires inside Carbon Nanotubes

Dan Liu, David Tománek*

Physics and Astronomy Department, Michigan State University, East Lansing, Michigan 48824, USA

Abstract

We propose a previously unexplored way to form Nb nanowires from NbCl_3 molecules inside carbon nanotubes (CNTs). We have studied this reaction by *ab initio* density functional calculations and found it to be catalytically promoted in presence of graphitic carbon. Our results suggest that chemisorption of NbCl_3 on the CNT is accompanied by a charge transfer of ≈ 0.5 electrons to the nanotube wall, which significantly weakens the Nb-Cl bond. We found that the bcc structure of Nb is not affected by the small diameter of the nanowire inside a CNT. We have also identified strong covalent bonds between the nanowires and the surrounding nanotube that are accompanied by a similar charge transfer of $\lesssim 0.5$ e from surface Nb atoms to the nanotube. The large electronic density of states of bulk Nb at E_F is not changed much in the confined geometry, suggesting that ultra-narrow nanowires of Nb may keep their superconducting behavior and form Josephson junctions in the quasi-1D geometry while being protected from the ambient by the enclosing CNT structure.

Keywords: Nanotube, carbon, CNT, catalyst, niobium, nanowire, superconductor, DFT

1. Introduction

Niobium holds a special place in the periodic table for several reasons. It is a ductile transition metal with a high melting temperature [1] $T_M = 2750$ K and the highest cohesive energy [1] $E_{coh} = 7.57$ eV/atom in the 4d transition metal series. Nb also displays the highest critical temperature $T_c = 9.25$ K among elemental superconductors [2, 3] and is unique with its ability to maintain an open body-centered cubic (bcc) structure until extremely high pressures [4] of hundreds of GPa. Nb is significantly harder than iron and an important constituent of thermally stable superalloys and superconducting alloys. There is strong interest in Nb nanowires covering applications ranging from efficient superconducting single-photon detectors [5, 6], Josephson tunnel junctions [7], and conductive fiber composites used as supercapacitors [8] and energy storage media [9]. A wide range of fabrication techniques including etching of sputter-deposited films [5] or compounds [9], templated electrodeposition [10], or deposition on nano-templates [11] were only capable of producing polycrystalline wires with diameters from 10-1000 nm. Availability of monocrystalline Nb nanowires

with only few nanometers in diameter is highly desirable especially for quantum applications in the superconducting regime. Yet the common synthesis approach based on high-temperature capillarity filling [12–20] of carbon nanotubes can not be used for Nb due to its high melting temperature, which is close to the stability limit of carbon nanotubes.

Here we propose a previously unexplored approach to synthesize Nb nanowires with a uniform diameter by heating up the NbCl_3 molecular crystal in presence of carbon nanotubes (CNTs) with a typical diameter $d \lesssim 2$ nm. The nanowires should form by decomposition of NbCl_3 inside CNTs at a temperature well below the melting point of Nb. In this process, the role of the CNT is threefold. First, the CNT is a template that defines the diameter of the enclosed. Second, graphitic carbon in the CNT acts as a catalyst, which lowers the temperature of converting NbCl_3 to metallic Nb and NbCl_5 to well below $1,000^\circ\text{C}$ [21]. Finally, the CNT protects the enclosed Nb nanowire from the ambient. We have performed *ab initio* density functional theory (DFT) calculations of the reaction mechanism and found that Nb nanowires may form in an activated exothermic process that involves a large number of atoms in concerted motion. The catalytic effect of a CNT originates in its ability to accept electrons from chemisorbed NbCl_3 . Our

*Corresponding author
 Email address: tomanek@pa.msu.edu (David Tománek)

calculations allow us to identify the optimum geometry of Nb nanowires that form inside the CNTs. Nb nanowires are faceted fragments of the bulk bcc structure with little reconstruction. They maintain the same high density of states at E_F as bulk Nb and thus should remain superconducting, similar to their bulk counterpart. More interesting, ultra-narrow Nb nanowire segments, separated by a narrow gap and held in place by the surrounding CNT, should form a Josephson junction in the quasi-1D geometry while being protected from the ambient by the enclosing CNT structure.

At first glance, formation of Nb nanowires inside carbon nanotubes should not appear surprising, since nanowires of other elements have been found inside CNTs [12–20]. So far, filling nanotubes by a metal [12] such as Pb had required initial melting of this metal, which subsequently entered the nanotubes by capillary action. Similar to other refractory metals, this approach fails for Nb with its melting point [1] $T_M = 2750$ K, which is close to the stability limit of carbon nanotubes between 951 K in presence of oxygen [22] and near 3,400 K in vacuum [23].

Our proposed approach is very different, as it involves sublimation of NbCl_3 molecules from a molecular crystal, their entry into the open end of a CNT and subsequent chemisorption on the inner wall. As we will discuss below, we find that chemisorption of NbCl_3 on the CNT wall is accompanied by a large charge transfer of 0.5 electrons from the molecule to the CNT, which strongly reduces the ionic charge of Cl atoms in this molecule. The charge redistribution in the adsorbed complex lowers the energy required to break the Nb-Cl bond by $\gtrsim 1$ eV. Consequently, the exothermic conversion of NbCl_3 to metallic Nb and NbCl_5 is promoted in presence of graphitic carbon, which plays the unusual role of a catalyst. There is preliminary experimental evidence [24] that formation of Nb nanowires inside CNTs from NbCl_3 is indeed possible at temperatures significantly lower than $1,000^\circ\text{C}$, which is required for this reaction to occur in vacuum, without a catalyst [21].

2. Computational results

We have considered different chlorides of niobium as potential precursors for metallic Nb and calculated the corresponding reaction energies by optimizing the initial and the final structures using *ab initio* DFT calculations. Among these, we found NbCl_5 to be unusually stable, as it forms spontaneously from metallic Nb and chlorine gas according to [25]

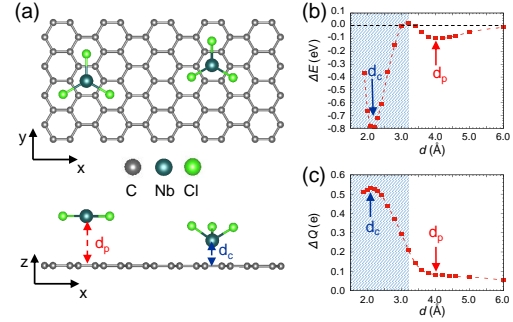
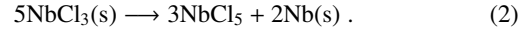


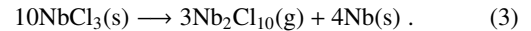
Figure 1: Interaction of an NbCl_3 molecule with a graphene monolayer. (a) Side and top views of the molecule at the distance $d = d_c$ and $d = d_p$ from graphene. (b) Interaction energy $\Delta E(d)$ between an NbCl_3 molecule and graphene. (c) Charge redistribution upon chemisorption of NbCl_3 on graphene.

The observed reaction energy [25, 26] of -797 kJ/mol or -8.26 eV per formula unit is in fair agreement with the calculated value of -7.48 eV. The strongly exothermic nature of this process indicates that the reverse process of forming metallic Nb from NbCl_5 is highly unlikely.

However, we found metallic Nb to form as one of the products of the decomposition of NbCl_3 according to [21, 27]



This reaction is exothermic and has been reported to occur at $1,000^\circ\text{C}$ under vacuum conditions [21, 27]. Even though NbCl_5 molecules are listed as one of the products, these molecules are known to dimerize spontaneously to $\text{Nb}_2\text{Cl}_{10}$. Then, Eq. (2) changes to



The calculated reaction energy of this exothermic process is $\Delta E = -19.82$ eV. Even though we know that this reaction does occur at $1,000^\circ\text{C}$, there is only limited information available about it due to its complexity [28], which involves continuous changes in the oxidation state of Nb. The reaction involves a concerted motion of 40 atoms in a 120-dimensional configuration space that is hard to search. Consequently, the reaction coordinate and transition states can not be characterized well, as we expand on in the Supplementary Material (SM).

According to Eq. (3), we consider NbCl_3 as a suitable precursor for the formation of metallic Nb. We note that this favorable precursor may also form by exposing NbCl_5 to hydrogen atmosphere according to [27]



This reaction is only slightly exothermic, with the reported reaction energy [27] of -35 kJ/mol. Even though we are unable to characterize the reaction coordinate, transition states and activation energies for the reaction in Eq. (3), we are still able to shed light on key steps in the reaction, which involves breaking of some and formation of other bonds in the Nb-Cl system, leading ultimately to metallic Nb inside a CNT.

In the first step, an NbCl_3 molecule adsorbs on the inner wall of the CNT, which we represent by a graphene monolayer in view of the low curvature of the 2-nm wide CNT. Our results are summarized in Fig. 1. Corresponding results for the interaction of NbCl_5 with graphene are presented in the SM.

As seen in Fig. 1(a), NbCl_3 is a planar molecule that prefers adsorption in the hollow site on graphene. The adsorption energetics is depicted in Fig. 1(b). NbCl_3 initially physisorbs at the distance $d_p = 4.07$ Å, gaining 0.10 eV in physisorption energy. Only a small energy barrier separates it from a much more stable chemisorbed state associated with an energy gain of 0.80 eV and a much smaller distance $d_c = 2.15$ Å from graphene. As shown in Fig. 1(a), the molecule deforms during the chemisorption, bringing the Nb atom closer to the surface. To better understand the changes in chemical bonding associated with the adsorption of NbCl_3 on graphene, we performed a single- ζ Mulliken population analysis of the system and monitored the net charge Q of NbCl_3 at different values of the adsorption distance d . We then defined the electron depletion $\Delta Q(d)$ on the molecule at distance d with respect to a desorbed molecule at $d = 10$ Å by $\Delta Q(d) = Q(d = 10 \text{ Å}) - Q(d)$. Our results in Fig. 1(c) indicate that the molecule remains almost neutral down to $d = d_p$, but loses up to 0.53 electrons as it approaches graphene in the chemisorbed state. From this viewpoint, graphene is not inert with respect to the chemical behavior of NbCl_3 .

As mentioned above, formation of metallic Nb from NbCl_3 molecules during the complex reaction behind Eq. (3) necessitates breaking or rearranging Nb-Cl bonds. Whereas separating a Cl atom from a free NbCl_3 molecule requires 4.57 eV, the same process requires only 2.60 eV when NbCl_3 is chemisorbed on graphene or inside a CNT. Also a related endothermic reaction that is likely to occur during the complex conversion process, where NbCl_3 first dimerizes to Nb_2Cl_6 and subsequently dissociates into NbCl_2 and NbCl_4 , requires 1.26 eV in vacuum and a significantly lower energy of 0.52 eV while adsorbed on graphitic carbon of a nanotube. Details of these particular reactions are presented in the SM.

We attribute the significant decrease of the reaction

energy barriers on graphitic carbon to the electron transfer from the chemisorbed molecule to the carbon nanotube. This catalytic effect is unusual, since with few exceptions [29, 30], graphitic carbon has been known to be catalytically inactive unless combined with another substance to form a graphene-based catalyst or a supported graphene catalyst. Consequently, formation of metallic Nb from NbCl_3 according to the reaction in Eq. (3) should occur inside a CNT at temperatures significantly lower than the reported value of 1,000°C in vacuum [21, 27]. This conjecture appears to be supported by preliminary experimental results [24].

Having established the possibility of forming metallic Nb inside a CNT, we now have to consider likely structures of finite-diameter Nb nanowires that are dynamically stable. Unlike in macroscopic structures including large-diameter wires, atomic packing may be significantly changed in nanostructures including nanowires due to the significant effect of surface tension that exerts compressive stress on the entire structure. We summarize observed and calculated values of the surface tension γ in Table 1. We have estimated the equivalent pressure for Nb nanowires in excess of 2 nm diameter and found it insufficient to convert the open bcc structure of bulk Nb to a more close-packed structure, in agreement with previous results [4]. We also cut out and optimized selected nanowires from bulk Nb(bcc) and found no signs of significant reconstruction. Thus, we believe that same as in the bulk, atoms in Nb nanowires are packed in the bcc structure, with possible atomic relaxations at the surface. The nanowires discussed in the following are to be considered stable dynamically, not only statically, since atomic rearrangement to a more stable structure has been excluded. Still, there is need to discuss possible shape changes at their faceted surface inside the nanotube void, which we do in the following.

Whereas the most stable structure would minimize the total surface energy in vacuum, it should minimize the total interface energy between Nb and the CNT in the Nb@CNT system. To obtain insight into the different components of the interface energy, we do not constrain our study to particular nanotube diameters, but rather study different Nb surfaces and their interaction with a graphene monolayer.

As a likely candidate for segments of the nanowire surface, we first consider the Nb(110) surface with the lowest value of γ according to Table 1. We would expect Nb nanowires with a surface consisting only of (110) facets to be most stable in vacuum. The interaction of the Nb(110) surface with graphene, representing a finite-diameter nanowire enclosed in a CNT, is presented in Fig. 2. Corresponding results for the Nb(100),

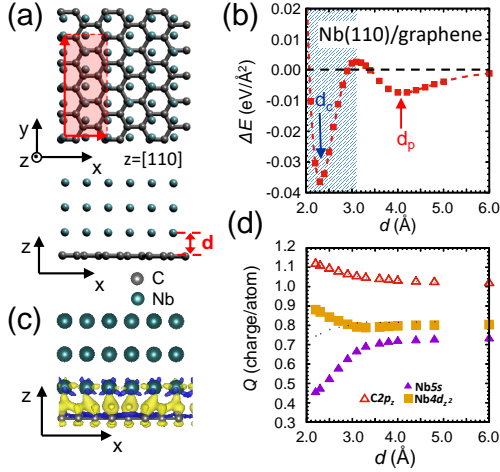


Figure 2: Interaction of the Nb(110) surface with a graphene monolayer. (a) Top and side views of the atomic arrangement, with the supercell highlighted by red. (b) Interaction energy ΔE between the Nb(110) surface and graphene as a function of the separation distance d . (c) Charge redistribution caused by the interaction of Nb(110) with graphene, superposed with the atomic structure. $\Delta\rho = \rho(\text{Nb/graphene}) - \rho(\text{Nb}) - \rho(\text{graphene})$ is shown by isosurfaces bounding regions of electron excess at $+4 \times 10^{-3} \text{ e}/\text{\AA}^3$ (yellow) and electron deficiency at $-4 \times 10^{-3} \text{ e}/\text{\AA}^3$ (blue). (d) Mulliken charge of specific atomic orbitals as a function of d .

Nb(111) and Nb(121) surfaces are presented in the SM. We represent the Nb(110) surface by a 3-layer slab.

Table 1: Characterization of selected Nb surfaces and their interaction with graphene based on DFT-PBE calculations. γ is the surface energy. The optimum Nb-graphene distance is d_c for chemisorption and d_p for physisorption. $\Delta E(d_c)$ is the Nb-graphene interaction energy and $\Delta Q(d_c)$ is the electron charge transferred from Nb to graphene at d_c , both given per area unit.

Surface	γ ($\text{eV}/\text{\AA}^2$)	d_c (\AA)	d_p (\AA)	$\Delta E(d_c)$ ($\text{eV}/\text{\AA}^2$)	$\Delta Q(d_c)$ ($\text{e}/\text{\AA}^2$)
(100)	0.152 0.142 ^a	2.32	-	0.035	0.040
(110)	0.127 0.129 ^a 0.155 ^b 0.159 ^c	2.31	4.07	0.037	0.048
(111)	0.150 0.146 ^a	2.28	-	0.022	0.031
(121)	0.146 0.146 ^a	2.37	-	0.025	0.032

^a Ref. [31].

^b Ref. [32].

^c Ref. [33].

Since Nb(110) is not epitaxial with the honeycomb lattice of graphene, we considered a large $\text{Nb}_{18}\text{C}_{16}$ supercell depicted in Fig. 2(a), which contained 16 C and 6 Nb atoms at the interface. Epitaxy, needed for the calculation, was enforced by compressing Nb(110) by 0.8% along the x -direction and stretching it by 2.1% along the y -direction, whereas graphene was left in its optimum structure. The Nb(110)/graphene interaction energy ΔE is plotted in Fig. 2(b) as a function of the interface distance d . Similar to the NbCl_3 molecule on graphene discussed above, we find two adsorption minima for this system. As also listed in Table 1, the shallower minimum, which we associate with physisorption, is characterized by $d_p = 4.07 \text{ \AA}$ and $\Delta E_p = -0.008 \text{ eV}/\text{\AA}^2$. The deeper minimum, which we associate with chemisorption, is characterized by $d_c = 2.31 \text{ \AA}$ and $\Delta E_c = -0.037 \text{ eV}/\text{\AA}^2$. These interaction energies are smaller than the surface energies listed in Table 1, but can not be ignored when discussing the surface structure of nanowires inside a CNT.

We find similarities in the interaction of graphene with the surface of Nb and a NbCl_3 molecule. Unlike in the physisorbed state of Nb on graphene, there is significant electron transfer from Nb to graphene in the more stable chemisorbed state. The spatial extent of this charge transfer is, however, limited to the one Nb layer closest to graphene, as shown in Fig. 2(c). To better understand the details of this charge transfer, we plotted the Mulliken population charge, obtained using a single- ζ basis, in Fig. 2(d) for atomic orbitals that were most affected. In graphene, it was the population of the $\text{C}2p_z$ orbital that increased at smaller interlayer distances. In Nb, the population of the $\text{Nb}4d_{z^2}$ state increased and that of the $\text{Nb}5s$ state decreased significantly at small interlayer distances. This confirms that the most significant bonding between Nb and C is associated with $pd\sigma$ bonding gaining strength over the $sp\sigma$ bond as Nb and C atoms approach each other. This bonding character is also reflected in the charge density redistribution in Fig. 2(c).

The interaction energies of different Nb surfaces with graphene are compared in Figs. 3(a)-3(c). Unlike for the (110) surface discussed above, there are no physisorption minima for Nb(100) and Nb(121) interacting with graphene. Among the three surfaces considered, Nb(110) interacts most strongly with graphene. The numerical values for the interaction energies of the different surfaces with graphene are summarized in Table 1.

Candidate structures for the most stable, $\approx 2 \text{ nm}$ -wide Nb nanowires are shown in Figs. 3(d)-3(f). Of these, the structure in Fig. 3(f) with a hexagonal cross-section

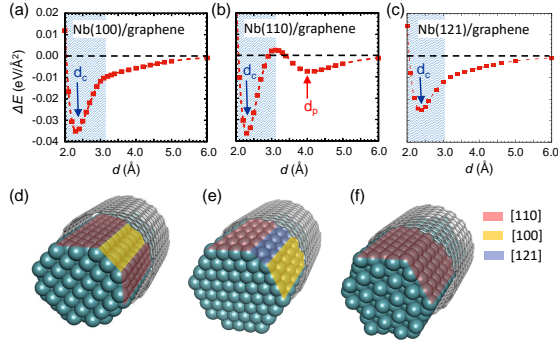


Figure 3: Interaction energy of (a) Nb(100), (b) Nb(110), and (c) Nb(121) with a graphene monolayer. These surfaces form facets on monocrystalline Nb nanowires. Most stable Nb nanowire geometries are shown schematically for nanowires with (d) (100) and (110), (e) (110), (121) and (100), and (f) only (110) facets.

is the most stable in vacuum, as it is terminated by [110] facets only. Since the Nb(110) surface interacts most strongly with graphene, this structure is favored even more strongly inside a CNT on energy grounds. In nanowires shown in Figs. 3(d) and 3(e), less stable [100] and [121] facets coexist with [110] facets, making these structures energetically less favorable in vacuum than that in Fig. 3(f). Since also the interaction of [100] and [121] facets with graphene is weaker than that of [110] facets, these structures remain energetically less favorable with respect to the structure in Fig. 3(f) also inside a CNT. We thus focus on the preferred structure in Fig. 3(f) in the following.

Finally, to estimate transport properties of Nb nanowires, we compare their electronic density of states (DOS) $N(E)$ to the infinite bcc structure in Fig. 4. We display schematically the bulk bcc structure in the top panel of Fig. 4(a), that of the nanowire of Fig. 3(f) in Fig. 4(b), and the same structure with edge atoms removed in Fig. 4(c). The DOS in the bottom panel of Fig. 4(a) reveals the metallic character of bulk Nb and reflects well the partial filling of the Nb4d band. The DOS of the two nanowires, shown in the bottom panels of Figs. 4(b) and 4(c) appears flatter near the Fermi level. Interestingly, the DOS value at E_F , $N(E_F)$, is essentially the same, possibly slightly higher in the nanowires than in the bulk structure. This would indicate that the conductivity of the nanowires should remain comparable to the bulk structure. We expect an electron transfer from the nanowires to the enclosing nanotube that involves only the outermost atoms in the nanowire. Depending on the nanowire diameter, the position of the Fermi level should be lowered

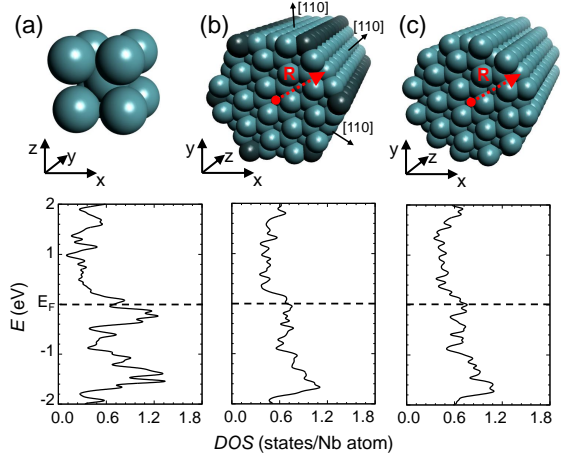


Figure 4: Electronic density of states (DOS) of (a) bulk Nb(bcc), (b) a Nb nanowire terminated by (110) facets, and (c) the Nb nanowire of (b) with atoms at the edges of the facets eliminated.

by $\lesssim 0.1$ eV with no effect on $N(E_F)$. The CNTs surrounding the nanowires may be intrinsically semiconducting or metallic and will contribute negligibly to the conductance of the system. In random samples, 2/3 of all single-wall CNTs are semiconducting.

Possibly more interesting than conducting behavior is the expected change in the critical temperature T_c for superconductivity. In BCS superconductors including Nb, T_c can be estimated using the McMillan equation [34]. The key quantities determining T_c are the Debye frequency ω_D and the electron-phonon coupling constant λ . Since the structure of the nanowires is essentially the same as that of their bulk counterpart, the vibrational spectra and thus ω_D should be the same. More important are changes in λ , which appears in the exponent of the expression for T_c . One factor in λ , namely the Bardeen-Pines interaction describing electron scattering by a phonon, should be the same in Nb nanowires and bulk Nb due to their similar electronic and phonon structure. The other factor in λ is $N(E_F)$, which we found to be essentially the same, if not higher, in the nanowires of Nb as in the bulk. Thus, we expect Nb nanowires down to 2 nm diameter to remain superconducting, with the same or possibly higher value of T_c than the 9.25 K value [2, 3] reported for bulk Nb.

3. Discussion

The CNTs play a triple role in our study. Besides their catalytic activity to lower the activation barrier for the decomposition of NbCl₃ and their function as a template

to form metallic Nb nanowires, they also protect these nanowires from the ambient.

A proper characterization of a chemical reaction involves identifying the reaction coordinate, the geometry and energy of transition states, and a detailed discussion of the dynamical stability of the final state structure. As we mentioned above, the reaction involves a concerted motion of 40 atoms in a 120-dimensional configuration space, which makes it impossible to search for the optimum transformation path between the initial and the final states, which we have characterized. We have also spent significant effort finding the optimum structure of nanowires that fill the void inside a given carbon nanotube. Of course, in absence of this steric constraint, the nanowires would decompose to the bulk Nb(bcc) metal, the most stable structure in the phase diagram of Nb. Clearly, many unknowns remain regarding the reaction details. Still, we have established that due to the catalytic activity of graphitic carbon, the reaction should run below 1,000°C, at which it had been observed under vacuum conditions.

The complex decomposition reaction of NbCl₃ leads not only to metallic Nb, but also to solid NbCl₅. The two bulk allotropes of NbCl₅ are wide-gap semiconductors and do not affect the electronic properties of the Nb nanowires, as we expand in more detail in the SM. We have also found that the interaction between NbCl₅ and the surrounding CNT wall is very weak and does not involve any charge transfer.

In a realistic sample, we may expect that the Nb nanowire may not be contiguous. Rather, finite-length Nb nanowire segments, which are held in place by the surrounding nanotube, may be separated by narrow gaps or short NbCl₅ segments along the axial direction of a CNT. Assuming that the surrounding CNT is semiconducting, the Nb-vacuum-Nb or Nb-NbCl₅-Nb structure may behave as a nanometer-wide, precisely controllable Josephson junction, the key component of future quantum computers. Besides its nanometer diameter, a significant advantage of a Nb-based Josephson junction would be its functionality up to $T_c(\text{Nb})=9$ K, a significant advantage over Al-based Josephson junctions that only operate below $T_c(\text{Al})=2$ K.

4. Summary and Conclusions

We have proposed a previously unexplored way to form Nb nanowires inside carbon nanotubes (CNTs) using not capillary filling by the metal, but rather filling the CNTs with NbCl₃ molecules, which decompose to metallic Nb and Nb₂Cl₁₀ molecules. We used *ab initio* density functional calculations to get insight into this

reaction, which turns out to be quite complex, as it involves a concerted motion of 40 atoms and Nb changing its oxidation state continuously. Whereas the reaction coordinate and associated activation barriers remain obscure, our calculations confirm that the reaction is strongly exothermic. Our finding that particular reaction steps are catalytically promoted in presence of graphitic carbon implies that the reaction temperature should decrease below 1,000°C required for it to run in vacuum. The same process could be used to form nanowires of other refractory metals including W with an even higher melting point. According to our calculations, chemisorption of NbCl₃ on the CNT is accompanied by a charge transfer of ≈ 0.5 electrons to the nanotube wall, which significantly weakens the Nb-Cl bond. We found that the bcc structure of Nb is not affected by the small diameter of the nanowire inside a CNT. We have also identified strong covalent bonds between the nanowires and the surrounding nanotube that are accompanied by a similar charge transfer of $\lesssim 0.5$ e from surface Nb atoms to the nanotube. We found that the large electronic density of states at E_F is not changed much in the confined geometry, suggesting that ultra-narrow nanowires of Nb may keep their superconducting behavior in the quasi-1D geometry while being protected from the ambient by the enclosing CNT structure. Under favorable conditions, Nb nanowire segments, separated by narrow gaps, may be held in place by the surrounding nanotube and form Josephson junctions operating at $T \lesssim T_c(\text{Nb})=9$ K.

5. Computational Techniques

Our calculations of the stability, equilibrium structure and electronic structure have been performed using density functional theory (DFT) as implemented in the SIESTA [35] code. Periodic boundary conditions have been used throughout the study, with 2D slabs or graphene and Nb represented by a periodic array of slabs separated by a 20 Å thick vacuum region. We also used a periodic array to represent 1D Nb nanowires separated by a 15 Å thick vacuum region. We used the Perdew-Burke-Ernzerhof (PBE) [36] exchange-correlation functional. The SIESTA calculations used norm-conserving Troullier-Martins pseudopotentials [37], a double- ζ basis including polarization orbitals, and a mesh cutoff energy of 250 Ry to determine the self-consistent charge density, which provided us with a precision in total energy of $\lesssim 2$ meV/atom. The reciprocal space has been sampled by a fine grid [38] of 7×3 k -points in the 2D Brillouin zones (BZ) of the supercells representing Nb/graphene

slabs. The 1D Brillouin zone of Nb nanowires has been sampled by 15 k -points. Geometries have been optimized using the conjugate gradient (CG) method [39], until none of the residual Hellmann-Feynman forces exceeded 10^{-2} eV/Å.

Acknowledgments

We thank Andrii Kyrylchuk for useful insight into the stability of Nb salts. We thank Yusuke Nakanishi and Zheng Liu for providing the initial idea for this study. We further appreciate scientific discussions about the synthesis of Nb nanowires with Katsumi Kaneko, Shuwen Wang, and Yung-Chang Lin. D.L. and D.T. acknowledge financial support by the NSF/AFOSR EFRI 2-DARE grant number EFMA-1433459. Computational resources have been provided by the Michigan State University High Performance Computing Center.

References

- [1] C. Kittel, Introduction to Solid State Physics, 7th Edition, Wiley, 2004.
- [2] B. T. Matthias, T. H. Geballe, V. B. Compton, Superconductivity, Rev. Mod. Phys. 35 (1963) 1–22.
- [3] D. K. Finnemore, T. F. Stromberg, C. A. Swenson, Superconducting properties of high-purity niobium, Phys. Rev. 149 (1966) 231–243.
- [4] P. F. Weck, J. P. Townsend, K. R. Cochrane, S. D. Crockett, N. W. Moore, Shock compression of niobium from first-principles, J. Appl. Phys. 125 (24) (2019) 245905.
- [5] A. J. Annunziata, O. Quaranta, D. F. Santavicca, A. Casaburi, L. Frunzio, M. Ejrnaes, M. J. Rooks, R. Cristiano, S. Pagano, A. Frydman, D. E. Prober, Reset dynamics and latching in niobium superconducting nanowire single-photon detectors, J. Appl. Phys. 108 (8) (2010) 084507.
- [6] C. M. Natarajan, M. G. Tanner, R. H. Hadfield, Superconducting nanowire single-photon detectors: physics and applications, Supercond. Sci. Technol. 25 (6) (2012) 063001.
- [7] M. D. Henry, S. Wolfley, T. Monson, R. Lewis, Ga lithography in sputtered niobium for superconductive micro and nanowires, Appl. Phys. Lett. 105 (7) (2014) 072601.
- [8] S. M. Mirvakili, M. N. Mirvakili, P. Englezos, J. D. W. Madden, I. W. Hunter, High-performance supercapacitors from niobium nanowire yarns, ACS Appl. Mater. & Interf. 7 (25) (2015) 13882–13888.
- [9] S. M. Mirvakili, A. Pazukha, W. Sikkema, C. W. Sinclair, G. M. Spinks, R. H. Baughman, J. D. W. Madden, Niobium nanowire yarns and their application as artificial muscles, Adv. Funct. Mater. 23 (35) (2013) 4311–4316.
- [10] K. Blagg, T. Greymountain, W. Kern, M. Singh, Template-based electrodeposition and characterization of niobium nanowires, Electrochem. Commun. 101 (2019) 39–42.
- [11] A. Rogachev, A. Bezryadin, Superconducting properties of polycrystalline nb nanowires templated by carbon nanotubes, Appl. Phys. Lett. 83 (3) (2003) 512–514.
- [12] P. M. Ajayan, S. Iijima, Capillarity-induced filling of carbon nanotubes, Nature 361 (6410) (1993) 333–334.
- [13] Y. Saito, T. Yoshikawa, Bamboo-shaped carbon tube filled partially with nickel, J. Cryst. Growth 134 (1) (1993) 154–156.
- [14] S. C. Tsang, Y. K. Chen, P. J. F. Harris, M. L. H. Green, A simple chemical method of opening and filling carbon nanotubes, Nature 372 (6502) (1994) 159–162.
- [15] J. Sloan, D. M. Wright, S. Bailey, G. Brown, A. P. E. York, K. S. Coleman, M. L. H. Green, J. Sloan, D. M. Wright, J. L. Hutchison, H.-G. Woo, Capillarity and silver nanowire formation observed in single walled carbon nanotubes, Chem. Commun. (1999) 699–700.
- [16] X. Fan, E. C. Dickey, P. C. Eklund, K. A. Williams, L. Grigorian, R. Buczko, S. T. Pantelides, S. J. Pennycook, Atomic arrangement of iodine atoms inside single-walled carbon nanotubes, Phys. Rev. Lett. 84 (2000) 4621–4624.
- [17] G.-H. Jeong, R. Hatakeyama, T. Hirata, K. Tohji, K. Motomiya, T. Yaguchi, Y. Kawazoe, Formation and structural observation of cesium encapsulated single-walled carbon nanotubes, Chem. Commun. (2003) 152–153.
- [18] A. García-Fuente, V. M. García-Suárez, J. Ferrer, A. Vega, Structure and electronic properties of molybdenum monatomic wires encapsulated in carbon nanotubes, J. Phys.: Cond. Matt. 23 (26) (2011) 265302.
- [19] T. Fujimori, R. dos Santos, T. Hayashi, M. Endo, K. Kaneko, D. Tománek, Formation and properties of selenium double-helices inside double-wall carbon nanotubes: experiment and theory, ACS Nano 7 (2013) 5607–5613.
- [20] H.-P. Komsa, R. Senga, K. Suenaga, A. V. Krasheninnikov, Structural distortions and charge density waves in iodine chains encapsulated inside carbon nanotubes, Nano Lett. 17 (6) (2017) 3694–3700.
- [21] R. Ripan, I. Ceteanu, Chimia metaleor, Vol. 2, Editura didactică și pedagogică, Bucharest, 1966, translated under the title *Neorganicheskaya khimia*, Moscow, Mir, 1972, vol. 2, p. 189.
- [22] H. Yu, C. Lu, T. Xi, L. Luo, J. Ning, C. Xiang, Thermal decomposition of the carbon nanotube/sio₂ precursor powders, J. Therm. Anal. Calorim. 82 (1) (2005) 97–101.
- [23] X. Wei, M.-S. Wang, Y. Bando, D. Golberg, Thermal stability of carbon nanotubes probed by anchored tungsten nanoparticles, Sci. Technol. Adv. Mater. 12 (4) (2011) 044605.
- [24] Yusuke Nakanishi, Yung-Chang Lin, Zheng Liu, Shuwen Wang, and Katsumi Kaneko (private communication).
- [25] E. Lavut, B. Timofeyev, V. Yuldasheva, G. Galchenko, Enthalpy of formation of niobium pentachloride, J. Chem. Thermodyn. 14 (6) (1982) 531–535.
- [26] P. Gross, C. Hayman, D. L. Levi, G. L. Wilson, The heats of formation of metal halides. niobium and tantalum pentachlorides, Trans. Faraday Soc. 56 (1960) 318–321.
- [27] S. Harjanto, A. Shibayama, K. Sato, G. Suzuki, T. Otomo, Y. Takasaki, T. Fujita, Thermal decomposition of nbcl₅ in reductive atmosphere by using hydrogen gas, Resour. Process. 52 (3) (2005) 113–121.
- [28] M. D. Korzyński, L. Braglia, E. Borfecchia, C. Lamberti, M. Dincă, Molecular niobium precursors in various oxidation states: An XAS case study, Inorg. Chem. 57 (21) (2018) 13998–14004.
- [29] W. Gu, J. Bai, B. Dong, X. Zhuang, J. Zhao, C. Zhang, J. Wang, K. Shih, Catalytic effect of graphene in bioleaching copper from waste printed circuit boards by acidithiobacillus ferrooxidans, Hydrometallurgy 171 (2017) 172–178.
- [30] X. Xu, Y. Liu, Z. Liu, F. Ke, C. Lin, K. Liu, Z. Zhang, Z. Hu, X. Li, X. Guo, Pristine graphene as a catalyst in reactions with organics containing C=O bonds, arXiv:1707.05607 (2017).
- [31] R. Tran, Z. Xu, B. Radhakrishnan, D. Winston, W. Sun, K. A. Persson, S. P. Ong, Surface energies of elemental crystals, Sci. Data 3 (2016) 160080.
- [32] K. C. Mills, Y. C. Su, Review of surface tension data for metallic elements and alloys: Part 1-pure metals, Int. Mater. Rev. 51 (6)

- (2006) 329–351.
- [33] E. N. Hodkin, M. G. Nicholas, D. M. Poole, The surface energies of solid molybdenum, niobium, tantalum and tungsten, *J. Less Common Met.* 20 (2) (1970) 93–103.
 - [34] W. L. McMillan, Transition temperature of strong-coupled superconductors, *Phys. Rev.* 167 (1968) 331–344.
 - [35] E. Artacho, E. Anglada, O. Dieguez, J. D. Gale, A. Garcia, J. Junquera, R. M. Martin, P. Ordejon, J. M. Pruneda, D. Sanchez-Portal, J. M. Soler, The siesta method; developments and applicability, *J. Phys. Cond. Mat.* 20 (6) (2008) 064208.
 - [36] J. P. Perdew, K. Burke, M. Ernzerhof, Generalized gradient approximation made simple, *Phys. Rev. Lett.* 77 (1996) 3865–3868.
 - [37] N. Troullier, J. L. Martins, Efficient pseudopotentials for plane-wave calculations, *Phys. Rev. B* 43 (1991) 1993.
 - [38] H. J. Monkhorst, J. D. Pack, Special points for brillouin-zone integrations, *Phys. Rev. B* 13 (1976) 5188–5192.
 - [39] M. R. Hestenes, E. Stiefel, Methods of conjugate gradients for solving linear systems, *J. Res. Natl. Bur. Stand.* 49 (1952) 409–436.

Supplementary Material for:

Catalytic Formation of Narrow Nb Nanowires Inside Carbon Nanotubes

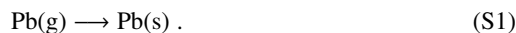
Dan Liu, David Tománek*

Physics and Astronomy Department, Michigan State University, East Lansing, Michigan 48824, USA

1. Reaction pathway

As mentioned in the main manuscript, Nb is a refractory metal with a high melting temperature $T_M = 2750$ K that is close to the decomposition temperature of carbon nanotubes (CNTs). Thus, capillary filling, which had been used for other elements with a much lower melting point, including Pb, can not be used for Nb.

Formation of Pb nanowires by capillary filling is a relatively straight-forward process, as it only involves the condensation of Pb atoms within the void inside a nanotube,



The reaction coordinate is the position of a single Pb atom in the 3-dimensional space and the reaction is thus easy to characterize.

For Nb, we propose a fundamentally different approach that yields metallic Nb as one of the products of a complex reaction that starts from the NbCl_3 molecular solid. As discussed in the main manuscript, this reaction is



With 40 atoms with 120 degrees of freedom involved, identifying the optimum reaction path in the 120-dimensional configuration space is practically impossible. Understanding this reaction is a serious challenge in Inorganic Chemistry.

We have attempted to run molecular dynamics simulations reflecting the reaction Eq. (S2) under high-pressure and high-temperature conditions to get guidance regarding the likely reaction path, but failed due to the limited simulation time. We have concluded that

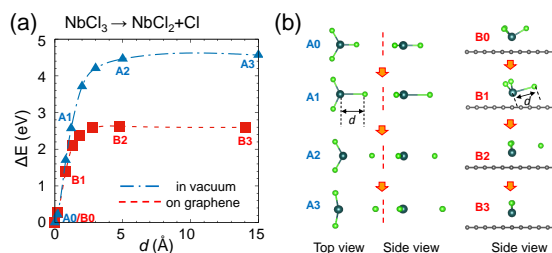


Figure S1: Dissociation of NbCl_3 to NbCl_2 and Cl according to Eq. (S3) in vacuum and on graphitic carbon. (a) Energetics of the reaction in vacuum (data points A0–A3, connected by the blue dash-dotted line) and on graphitic carbon (data points B0–B3, connected by the red dashed line). (b) Snap shots of the intermediate geometries. The reaction coordinate is represented by d , the length of one particular Nb-Cl bond.

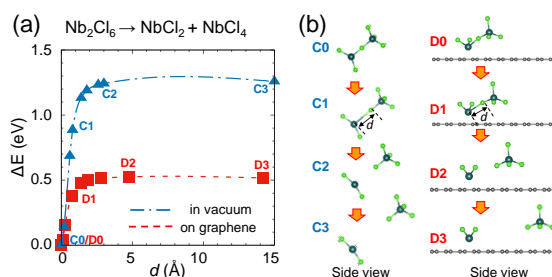


Figure S2: Transformation of Nb_2Cl_6 to NbCl_2 and NbCl_4 according to Eq. (S4) in vacuum and on graphitic carbon. (a) Energetics of the reaction in vacuum (data points C0–C3, connected by the blue dash-dotted line) and on graphitic carbon (data points D0–D3, connected by the red dashed line). (b) Snap shots of the intermediate geometries. The reaction coordinate is represented by d , the length of one particular Nb-Cl bond.

locating intermediate structures and transition states for a reaction as complex as in Eq. (S2) is not feasible computationally.

Still, we can provide results of limited calculations for processes that likely take place during the complex reaction in Eq. (S2), both in vacuum and inside a carbon

*Corresponding author
Email address: tomanek@pa.msu.edu (David Tománek)

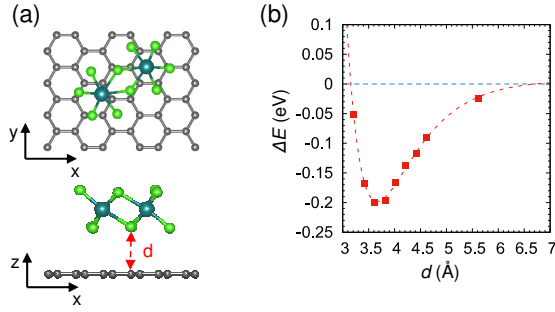


Figure S3: Interaction of an Nb₂Cl₁₀ molecule with a graphene monolayer. (a) Side and top views of the molecule at the distance d from graphene. (b) Interaction energy $\Delta E(d)$ between an Nb₂Cl₁₀ molecule and graphene.

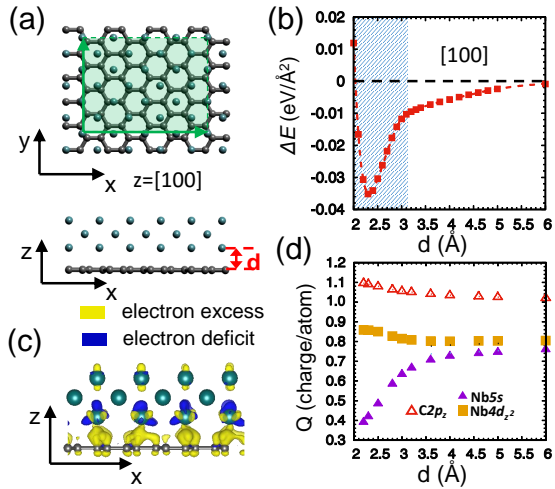
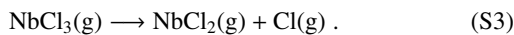


Figure S4: Interaction of the Nb(100) surface with a graphene monolayer. (a) Top and side views of the atomic arrangement, with the supercell highlighted by red. (b) Interaction energy ΔE between the Nb(100) surface and graphene as a function of the separation distance d . (c) Charge redistribution caused by the interaction of Nb(100) with graphene, superposed with the atomic structure. $\Delta\rho = \rho(\text{Nb/graphene}) - \rho(\text{Nb}) - \rho(\text{graphene})$ is shown by isosurfaces bounding regions of electron excess at $+4 \times 10^{-3} \text{ e}/\text{\AA}^3$ (yellow) and electron deficiency at $-4 \times 10^{-3} \text{ e}/\text{\AA}^3$ (blue). (d) Mulliken charge of specific atomic orbitals as a function of d .

nanotube.

One reaction step that is likely to occur in this complex reaction is the detachment of a chlorine atom from an NbCl₃ molecule of the starting substance according to



The energetics of the corresponding endothermic dissociation process, which may occur in vacuum or on

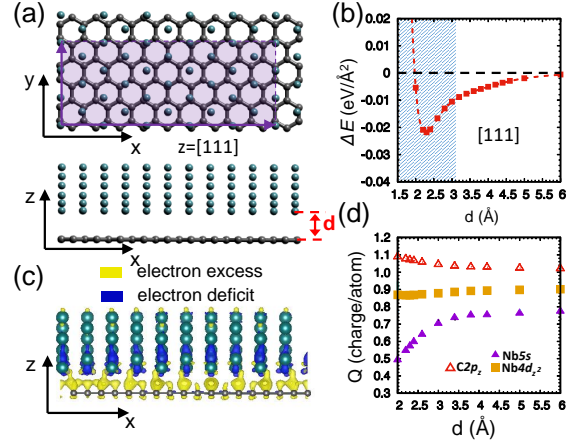
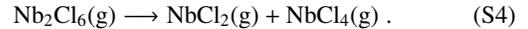


Figure S5: Interaction of the Nb(111) surface with a graphene monolayer. (a) Top and side views of the atomic arrangement, with the supercell highlighted by red. (b) Interaction energy ΔE between the Nb(111) surface and graphene as a function of the separation distance d . (c) Charge redistribution caused by the interaction of Nb(111) with graphene, superposed with the atomic structure. $\Delta\rho = \rho(\text{Nb/graphene}) - \rho(\text{Nb}) - \rho(\text{graphene})$ is shown by isosurfaces bounding regions of electron excess at $+4 \times 10^{-3} \text{ e}/\text{\AA}^3$ (yellow) and electron deficiency at $-4 \times 10^{-3} \text{ e}/\text{\AA}^3$ (blue). (d) Mulliken charge of specific atomic orbitals as a function of d .

graphitic carbon, is presented in Fig. S1 along with the corresponding geometries. Clearly, the dissociation energy is lowered significantly in presence of graphitic carbon.

Another reaction likely to occur during the conversion of NbCl₃ to metallic Nb and other molecules is the dimerization of NbCl₃ to Nb₂Cl₆, followed by simultaneous detachment of a Cl atom from NbCl₃ while a new Nb-Cl bond is being formed with another NbCl₃ molecule. One reaction that reflects simultaneous dissociation and formation of an Nb-Cl bond is



The energetics of this endothermic dissociation process, which may occur in vacuum or on graphitic carbon, is illustrated in Fig. S2 along with the corresponding geometries. Clearly, the energy barrier is lowered in presence of graphitic carbon also for this reaction.

2. Interaction of NbCl₅ with graphene

NbCl₅ dimerizes to Nb₂Cl₁₀ molecules shown in Figure S3(a). In contrast to NbCl₃ discussed in the main manuscript, there is only one shallow ‘physisorption’ state of Nb₂Cl₁₀ on graphene, as seen in Figure S3(b). The physisorption energy $\Delta E = -0.2 \text{ eV}$ is

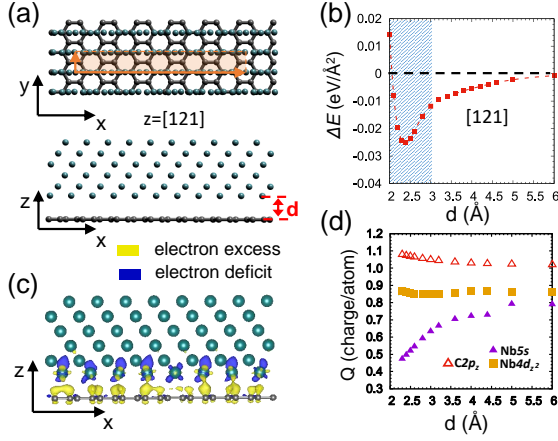


Figure S6: Interaction of the Nb(121) surface with a graphene monolayer. (a) Top and side views of the atomic arrangement, with the supercell highlighted by red. (b) Interaction energy ΔE between the Nb(121) surface and graphene as a function of the separation distance d . (c) Charge redistribution caused by the interaction of Nb(121) with graphene, superposed with the atomic structure. $\Delta\rho = \rho(\text{Nb/graphene}) - \rho(\text{Nb}) - \rho(\text{graphene})$ is shown by isosurfaces bounding regions of electron excess at $+4 \times 10^{-3} \text{ e}/\text{\AA}^3$ (yellow) and electron deficiency at $-4 \times 10^{-3} \text{ e}/\text{\AA}^3$ (blue). (d) Mulliken charge of specific atomic orbitals as a function of d .

very small and the charge transfer between the molecule and graphene is negligible.

3. Interaction of Nb(100), Nb(111) and Nb(121) surfaces with graphene

An analogy to the results for interaction of Nb(110) with graphene, presented in Figure 3 of the main manuscript, we present results for graphene interacting with Nb(100) in Figure S4, Nb(111) in Figure S5, and Nb(121) in Figure S6.

4. Electronic structure of bulk NbCl₅

We have optimized the bulk structure of two bulk allotropes of NbCl₅ using density functional theory (DFT) as specified in the main manuscript. We have found their energies to differ by *less than 1* meV per formula unit, indicating that the two allotropes are equally stable. We present the DFT-based electronic density of states (DOS) in Fig. S7. In view of the fact the DFT eigenvalues always underestimate the fundamental band gap, both allotropes are clearly wide-gap semiconductors.

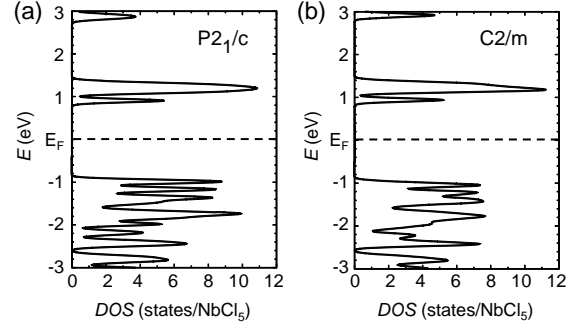


Figure S7: Electronic density of states (DOS) of two monoclinic bulk allotropes of niobium pentachloride. (a) NbCl₅ with $P2_1/c$ symmetry and 24 atoms in total per unit cell. (b) NbCl₅ with $C2/m$ symmetry and 72 atoms in total per unit cell. Both crystals are wide-gap semiconductors.